



# Multi-strange baryon production in pp, p–Pb and Pb–Pb collisions measured with ALICE at the LHC.

Didier Alexandre (for the ALICE Collaboration)<sup>1</sup>

*University of Birmingham, United Kingdom*

*E-mail: [didier.alexandre@cern.ch](mailto:didier.alexandre@cern.ch)*

---

## Abstract

Multi-strange baryons are of particular interest in the understanding of particle production mechanisms, as their high strangeness content makes them susceptible to changes in the hadrochemistry of the colliding systems. In ALICE, these hyperons are reconstructed via the detection of their weak decay products, which are identified through their measured ionisation losses and momenta in the Time Projection Chamber. The production rates of charged  $\Xi$  and  $\Omega$  baryons in proton-proton (pp), proton-lead (p–Pb) and lead-lead (Pb–Pb) collisions are reported as a function of  $p_T$ . A direct comparison in the hyperon-to-pion ratios between the three collision systems is made as a function of event charged-particle multiplicity. The recently measured production rates in p–Pb interactions reveal an enhancement with increasing event multiplicity, consistent with a hierarchy dependent on the strangeness content of the hyperons. These results are discussed in the context of chemical equilibrium predictions, taking into account the extracted temperature parameter from a thermal model fit to the hadron yields in Pb–Pb data.

*Keywords:* Multi-strange baryons, Strangeness enhancement, Chemical equilibrium, Radial flow

---

## 1. Introduction

In pp collisions, the production of strange particles is limited by the local canonical strangeness conservation law. This is not the case in central heavy-ion collisions, where strange quarks are expected to be produced more abundantly, which is translated to an enhanced formation of strange baryons after hadronisation [1, 2]. In addition, the partial restoration of the chiral symmetry at the expected QCD phase transition in A–A collisions lowers the energy threshold for strangeness production to the level of the bare strange quark mass, a value which is comparable to the temperatures achieved in such energetically dense environments. For these reasons, the measurement of the charged multi-strange  $\Xi$  and  $\Omega$  hyperons is an observable very sensitive to the early stages of the collision system, and therefore interesting for the understanding of strongly interacting matter in different collision conditions.

The phenomenon of strangeness enhancement in heavy-ion collisions with respect to pp (p–Be) collisions has been observed with Pb–Pb interactions at the NA57 experiment [3], at STAR [4] with Au–Au collisions, and confirmed by ALICE in central 2.76 TeV Pb–Pb collisions [5]. The chemical saturation values for the  $\Xi/\pi$  and  $\Omega/\pi$  ratios<sup>2</sup> extracted from global fits to hadron yields in Au–Au collisions at STAR with the grand canonical approach appeared to

---

<sup>1</sup>A list of members of the ALICE Collaboration and acknowledgements can be found at the end of this issue.

<sup>2</sup> $\Xi/\pi$  and  $\Omega/\pi$  refer to the ratio of particle and anti-particle sums.

be consistent with the ALICE central Pb–Pb results within systematic errors for an equilibrium temperature of  $T=164$  MeV [6]. However, the same model overpredicted the measured  $(p + \bar{p})/(\pi^- + \pi^+)$  values by about 50%. A lower chemical freeze-out temperature of 156 MeV was obtained from the global fit to the measured Pb–Pb hadron yields [7].

ALICE has recently measured the multi-strange baryon production in the intermediate p–Pb reference system as a function of charged-particle multiplicity. In this conference proceeding, a description of the method of identifying multi-strange baryons in p–Pb collisions is given, the  $p_T$  spectra of these particles are presented and the hyperon-to-pion integrated yield ratios are explored as a function of multiplicity in the three collision types. In addition, these ratios at high multiplicity are compared to the chemical equilibrium predictions with the grand canonical assumption.

## 2. Detection of multi-strange particles in p–Pb collisions with ALICE

With an overall branching ratio of 63.9% (43.3%),  $\Xi^-$  ( $\Omega^-$ ) baryons weakly decay into a  $\pi^-$  ( $K^-$ ) and a  $\Lambda$ , which itself decays into a  $p\pi^-$  pair.<sup>3</sup> The tracks formed by the daughter particles of these decays, are reconstructed in the Inner Tracking System and in the large Time Projection Chamber (TPC), and the particle identity is determined through the measured ionisation losses and momenta measured in the TPC.

To reduce the combinatorial background in the selection of the weakly decaying multi-strange particles ('cascades'), a set of geometrical cuts based on the decay topologies were applied: minimum transverse radial distances of the cascade and corresponding  $\Lambda$  ('V0') decay vertices form the Primary Vertex (PV) were set as part of the selection criteria, as well as minimal Distances of Closest Approach (DCA) between each final state particle track and the PV. Upper limit cuts were set on the DCA between the V0 decay tracks and between the V0 and the bachelor track. In addition, a cut on the cosine of pointing angle - angle between the line connecting the PV to the decay vertex and the reconstructed momentum vector of the decaying particle - of the  $\Xi^-$  and of the daughter  $\Lambda$  of  $> 0.97$  was applied.

The signal was extracted from the invariant mass distributions produced with the selected cascade candidates. In every  $p_T$  bin, a Gaussian function was fit to the mass peak and a central area defined within  $-4\sigma$  and  $4\sigma$  of that peak. The candidate counts in two background bands defined in the intervals  $[-8;-4]\sigma$  and  $[4;8]\sigma$  from the Gaussian peak were subtracted from the entries in the central bins to give the signal.

The  $p_T$  spectra of the multi-strange particles were measured in seven different multiplicity classes. The multiplicity percentile of each event was obtained from the amplitude distribution of the forward V0A detector (placed within the pseudorapidity range  $2.8 < \eta < 5.1$ , on the outgoing Pb-beam side). This avoided measuring the multiplicity in the same mid-rapidity region of the detector as the region where the multi-strange particles were measured (within the rapidity range  $-0.5 < y < 0.0$  in the centre-of-mass system of the collision system, and each daughter track within  $|\eta_{lab}| < 0.8$ ), and possible selection biases it could cause. The averaged charged-particle pseudorapidity densities with respect to which the integrated multi-strange yields were studied, were measured in the central  $|\eta_{lab}| < 0.5$  detector region in each of the V0A -determined multiplicity classes.

## 3. Results

The measured  $p_T$  distributions ranging between 0.6 (0.8) and 7.2 (5.0) GeV/c for  $\Xi^-$  ( $\Omega^-$ ) are shown in Figure 1 as a function of multiplicity. A hardening of the spectra with multiplicity can be observed in the shape of the curves both for  $\Xi^-$  and  $\Omega^-$ . Moreover, the central  $\Xi^-$  and  $\Omega^-$  p–Pb spectra have been shown to fit the hydrodynamics-based Blast Wave (BW) function [8] simultaneously with the other hadrons, yielding kinetic freeze-out temperature and mean expansion velocity  $< \beta_T >$  parameters in agreement with those already published without the multi-strange particles [9]. This hints at a collective behaviour of the hyperons after the collision, consistent with the radial flow interpretation

<sup>3</sup>In the rest of this document,  $\Xi^-$  and  $\Omega^-$  will implicitly refer to both particle and antiparticle.

from the  $p$ ,  $\pi$ ,  $K$  and  $\Lambda$  production study in p–Pb [5] and in Pb–Pb collisions [10, 11]. Therefore a full-range BW fit was used to extract the integrated yields and extrapolate the  $p_T$  distributions down to 0 GeV/c. While the  $\Xi^-$  ( $\Omega^-$ ) spectrum extrapolation fractions of the yields amount to about 25% (40%) in the lowest multiplicity classes (80–100% percentile bands), the obtained errors due to the extrapolation technique are of no more than 5% (15%) in those bins.

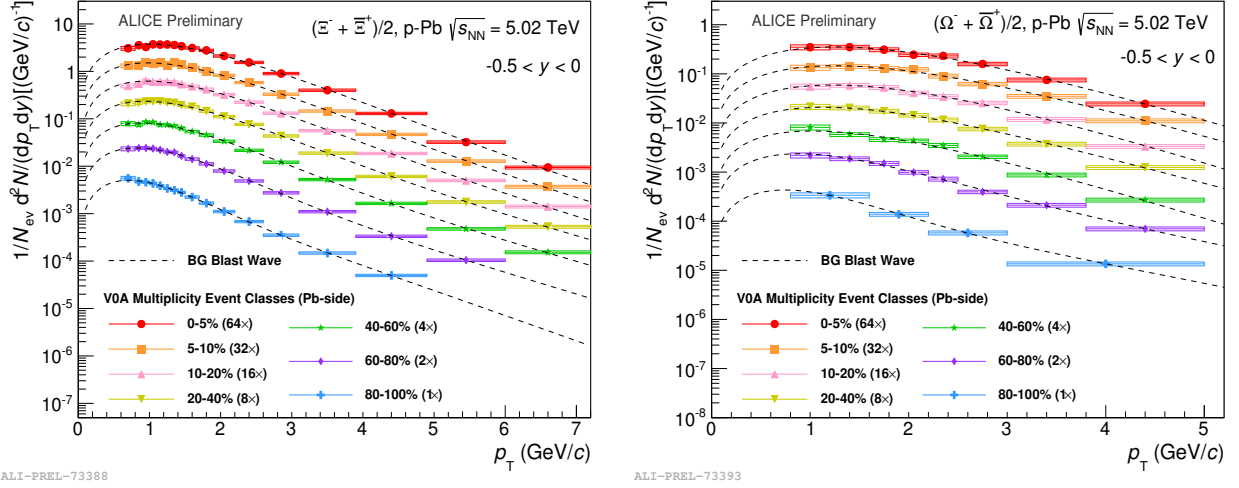


Figure 1. Charged  $\Xi$  and  $\Omega$   $p_T$  spectra in seven multiplicity classes. The average spectra of particle and anti-particle are shown.

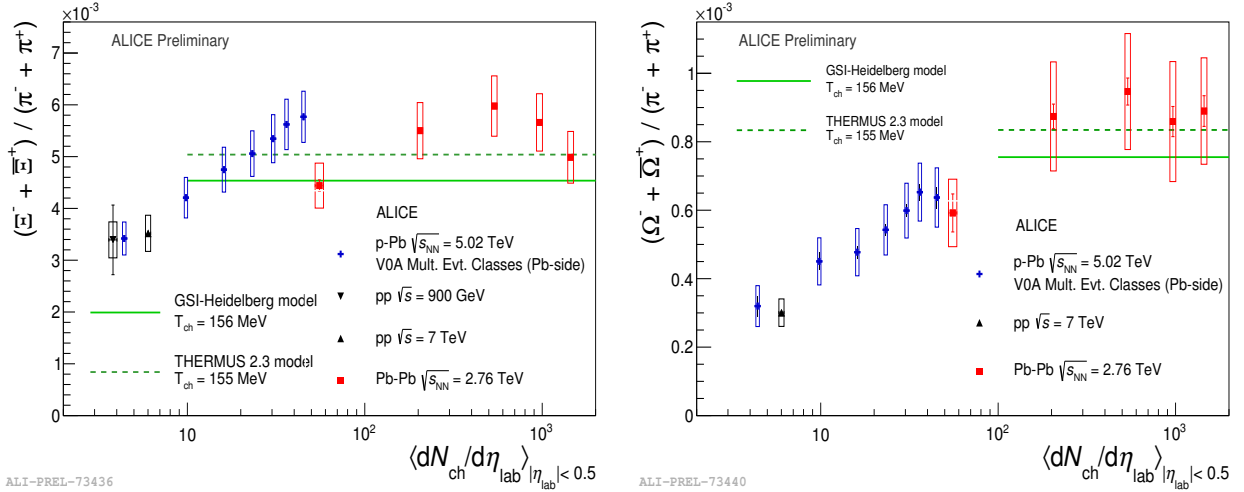


Figure 2.  $(\Xi^- + \Xi^+)/(\pi^- + \pi^+)$  and  $(\Omega^- + \Omega^+)/(\pi^- + \pi^+)$  ratios as a function of charged-particle pseudorapidity density in pp, p–Pb and Pb–Pb collisions measured by ALICE.

Figure 2 shows the recently measured p–Pb hyperon-to-pion ratios as a function of  $\langle dN_{ch}/d\eta \rangle_{|\eta_{lab}| < 0.5}$ , compared with pp and Pb–Pb measurements. The p–Pb data were taken in a multiplicity range of over one order of magnitude and intermediate between the other two collision systems. An enhancement of the multi-strange baryons with multiplicity in p–Pb data is observed, the effect being stronger for  $\Omega$  baryons, for which the enhancement factor in high with respect to low multiplicity events is roughly 2. In fact, together with the earlier  $2\Lambda/(\pi^- + \pi^+)$  ratios published in [9], one observes a consistent enhancement hierarchy in p–Pb dependent on the strangeness quantum number of the

baryon.

The solid and dashed green lines in Figure 2 represent the grand canonical limits for chemical saturation resulting from the global fits to ALICE Pb–Pb data. Two different model limits are shown - the GSI-Heidelberg model [12], and the THERMUS model [13] - with extracted chemical equilibrium temperatures of  $156 \pm 1.5$  MeV and  $155 \pm 2.0$  MeV, respectively [14]. Except for the most peripheral Pb–Pb data point, the saturation limits tend to overlap with the lower end of the error bars of the Pb–Pb data points or lie below them. In p–Pb, the  $\Xi/\pi$  ratios in high multiplicity events agree with those observed in non-peripheral Pb–Pb measurements. This stands in contrast to the Omega-to-pion ratios, which lie below the values observed in the most central Pb–Pb collisions. Consequently, the  $\Omega/\pi$  ratio does not reach the equilibrium level suggested by the data.

#### 4. Conclusions

The production of the multi-strange  $\Xi^-$  and  $\Omega^-$  baryons and their antiparticles was measured in p–Pb collisions with the ALICE detector in seven different event multiplicity bins. A hardening in the shape of the extracted  $p_T$  distributions with increasing multiplicity was observed, consistent with the interpretation of increasing radial flow velocity. A clear strangeness enhancement with respect to the pion production was measured in p–Pb collisions for these hadrons as a function of charged-particle multiplicity. The p–Pb data points bridge the ratio values in pp to those in Pb–Pb. A theoretical description of this transition will improve our understanding of strangeness production in high energy collisions. The chemical equilibrium temperature parameter obtained from the simultaneous fit to the hadron yields measured in ALICE Pb–Pb collisions is lower than the one extracted at STAR with Au–Au data and lies at about 156 MeV. While the  $\Omega/\pi$  ratio in p–Pb approaches this saturation level with increasing multiplicity, the high multiplicity  $\Xi/\pi$  values are comparable to those in central Pb–Pb data and lie above the estimated saturation limits.

#### References

- [1] F. Becattini, An Introduction to the Statistical Hadronization Model. [arXiv:0901.3643](#).
- [2] B. M. J. Rafelski, Strangeness production in the quark-gluon plasma, *Physics Review Letters* 48 (16) (1982) 1066–1069.
- [3] F. Antinori, et al., Strangeness enhancements at central rapidity in 40 A GeV/c Pb-Pb collisions, *J.Phys.* G37 (2010) 045105. [arXiv:1001.1884](#), [doi:10.1088/0954-3899/37/4/045105](#).
- [4] B. Abelev, et al., Enhanced strange baryon production in Au + Au collisions compared to p + p at  $\sqrt{s_{NN}} = 200$ -GeV, *Phys.Rev.* C77 (2008) 044908. [arXiv:0705.2511](#), [doi:10.1103/PhysRevC.77.044908](#).
- [5] B. B. Abelev, et al., Multi-strange baryon production at mid-rapidity in Pb-Pb collisions at  $\sqrt{s_{NN}} = 2.76$  TeV, *Phys.Lett.* B728 (2014) 216–227. [arXiv:1307.5543](#), [doi:10.1016/j.physletb.2013.11.048](#).
- [6] B. Abelev, et al., Centrality dependence of  $\pi$ , K, p production in Pb-Pb collisions at  $\sqrt{s_{NN}} = 2.76$  TeV, *Phys.Rev.* C88 (4) (2013) 044910. [arXiv:1303.0737](#), [doi:10.1103/PhysRevC.88.044910](#).
- [7] J. Stachel, A. Andronic, P. Braun-Munzinger, K. Redlich, Confronting LHC data with the statistical hadronization model, *J.Phys.Conf.Ser.* 509 (2014) 012019. [arXiv:1311.4662](#), [doi:10.1088/1742-6596/509/1/012019](#).
- [8] E. Schnedermann, J. Sollfrank, U. W. Heinz, Thermal phenomenology of hadrons from 200-A/GeV S+S collisions, *Phys.Rev.* C48 (1993) 2462–2475. [arXiv:nuc1-th/9307020](#), [doi:10.1103/PhysRevC.48.2462](#).
- [9] B. B. Abelev, et al., Multiplicity Dependence of Pion, Kaon, Proton and Lambda Production in p-Pb Collisions at  $\sqrt{s_{NN}} = 5.02$  TeV, *Phys.Lett.* B728 (2014) 25–38. [arXiv:1307.6796](#), [doi:10.1016/j.physletb.2013.11.020](#).
- [10] B. Abelev, et al., Pion, Kaon, and Proton Production in Central Pb–Pb Collisions at  $\sqrt{s_{NN}} = 2.76$  TeV, *Phys.Rev.Lett.* 109 (2012) 252301. [arXiv:1208.1974](#), [doi:10.1103/PhysRevLett.109.252301](#).
- [11] B. B. Abelev, et al.,  $K_S^0$  and  $\Lambda$  production in Pb-Pb collisions at  $\sqrt{s_{NN}} = 2.76$  TeV, *Phys.Rev.Lett.* 111 (22) (2013) 222301. [arXiv:1307.5530](#), [doi:10.1103/PhysRevLett.111.222301](#).
- [12] A. Andronic, P. Braun-Munzinger, J. Stachel, Thermal hadron production in relativistic nuclear collisions: The Hadron mass spectrum, the horn, and the QCD phase transition, *Phys.Lett.* B673 (2009) 142–145. [arXiv:0812.1186](#), [doi:10.1016/j.physletb.2009.02.014](#), [doi:10.1016/j.physletb.2009.06.021](#).
- [13] S. Wheaton, J. Cleymans, THERMUS: A Thermal model package for ROOT, *Comput.Phys.Commun.* 180 (2009) 84–106. [arXiv:hep-ph/0407174](#), [doi:10.1016/j.cpc.2008.08.001](#).
- [14] M. Floris, Hadron yields and the phase diagram of strongly interacting matter. [arXiv:1408.6403](#), [doi:10.1016/j.nuclphysa.2014.09.002](#).